SAND2020-5746C

Characterization of DC Arc-Plasmas Generated by High-Voltage Photovoltaic Power Systems

Caroline Winters
Sandia National Laboratories
Albuquerque, USA
cwinte@sandia.gov

Alvaro Cruz Cabrera
Sandia National Laboratories
Albuquerque, USA
aacruzc@sandia.gov

Kenneth Armijo
Sandia National Laboratories
Albuquerque, NM
kmarmij@sandia.gov

***Abstract*— Field tests of air-copper arcs were completed at a high-voltage, photovoltaic power plant using a simplified, "arc-in-a-box" geometry to study dc arc faults. Copper electrodes, 12.7 mm in diameter, were arranged in three configurations and an arc was initiated using < 700 V_{DC} with applied energy varying from 40-3900 kJ. Constitutive modeling of the arc-discharge predicts arc temperatures much greater than 1000 K. Two diagnostic techniques were fielded to characterize the spectral and thermal emission. Optical emission spectroscopy determined the time-resolved and mean arc temperatures were approximately T_{mean} = 7500 with standard deviations of ± 600 K, and IR imaging mapped the mean temperature field, T_{mean} = 1500 K, of the arc-heated environment.**

Keywords—Optical Emission Spectroscopy, IR imaging, dc arcs, high energy arc faults

I. Introduction

A dc arc fault occurs when the potential between two current-carrying conductors, or electrodes, reaches the threshold to ionize the surrounding air. The resulting plasma is sustained by an unabated, continuous current flow, until it is interrupted by an upstream over□current protective device or energy absorbing body. Arc faults release enormous amounts of energy, resulting in high temperatures and other hazards, shown in Figure 1.

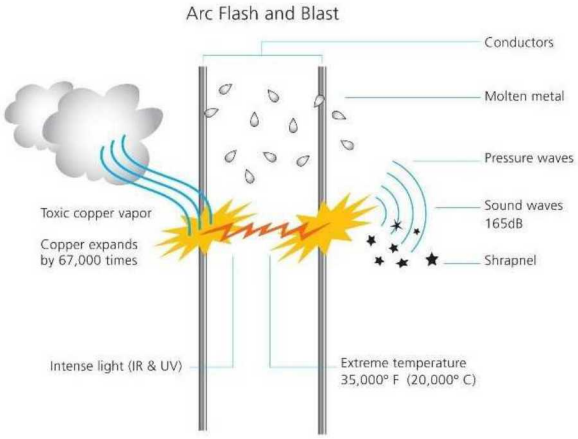

Fig. 1. Schematic of an arc fault outlining its potential damaging effects [1].

Sandia National Laboratories is a multimission laboratory managed and operated by National Technology & Engineering Solutions of Sandia, LLC, a wholly owned subsidiary of Honeywell International Inc., for the U.S. Department of Energy's National Nuclear Security Administration under contract DE-NA0003525.

Recently, 1,500 V_{DC} products have been allowed onto the market. To understand and predict the incident energy released from a high-voltage, arc fault event, Sandia National Laboratories (SNL) has developed a localized arc-plasma model, in collaboration with the Electric Power Research Institute (EPRI), which considers constitutive equations describing voltage breakdown across a spark gap and the thermal-fluidic phenomena that gives rise to incident energy over a zone of influence (ZOI) during an arc-flash event. This work is based on a prior arc-discharge model, which estimated arc temperatures greater than T = 1000 K, for arc currents higher than I = 10 A [2]. These predicted temperatures increase with the addition of vaporized metal from the electrodes. In an arc-flash event, these temperatures could be high enough to super heat the air, as well as melt and/or vaporize the materials the plasma contacts. Model validation, therefore, requires a suite of diagnostics capable of surviving the arc-flash environment, while measuring the quantities of interest during field testing.

II. Experimental Design

A. *"Arc-in-a-box" Field Testing*

EPRI and SNL conducted field experiments at a Detroit Edison (DTE) PV plant in July 2019. Here, the site consisted of a 35 MW_{DC} (1,000 Vdc, rated) solar farm in the Detroit, MI Area, which was selected considering the higher voltage levels operated at the PV facility, shown in Figure 2.

Fig. 2. Image of the test set-up at the Detroit Edison (DTE) PV Plant.

The tests were intended to measure incident energy, arc-voltage, arc-current, arc-flash movement, thermal emission, irradiance and arc-temperature.

Test boxes, 50.8 cm x 50.8 cm x 50.8 cm, were constructed with an open front to allow optical access of the 12.7 mm diameter copper electrodes set in three configurations: vertical pin-to-pin, vertical parallel, and horizontal pin-to-pin, shown in Figure 3. Copper bridge wire was placed across the electrodes to initiate the fault, allowing a current increase to lead to ionization between the two electrodes.

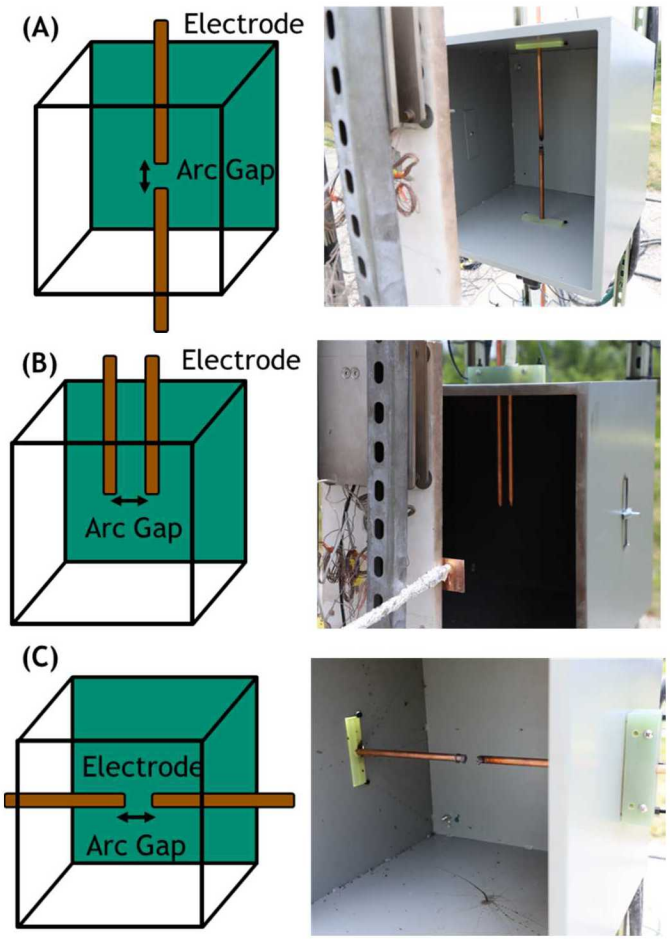

Fig. 3. Schematic and image of the "arc-in-a-box" test configurations: A) vertical pin-to-pin, B) vertical, parallel, and C) horizontal, pin-to-pin, which were run with two copper electrodes of 12.7 mm diameter.

Up to eight combiner boxes provided an input source of $V > 700$ V_{DC} and varying energies. The gap spacing of the electrodes was varied between $G = 12.7$ mm and 152.4 mm, to vary the breakdown voltage necessary for arc initiation. The full set of test conditions is provided in Table 1.

TABLE I. TEST CONDITIONS

Electrode Orientation	Gap (in)	Applied Energy (kJ)	Test duration (s)
Horizontal, pin-to-pin	0.5	103	2
Horizontal, pin-to-pin	2.0	494	2
Horizontal, pin-to-pin	4.0	604	2
Horizontal, pin-to-pin	6.0	685	2
Vertical, parallel	0.5	713	2
Vertical, parallel	0.5	653	2
Vertical, parallel	0.5	885	2
Vertical, parallel	2.0	768	2
Vertical, parallel	2.0	3937	10
Vertical, pin-to-pin	0.5	40	2
Vertical, pin-to-pin	2.0	50	2

The predicted incident energy using the fabricated modules was found to be within -15.5% to +13% of the measured values for a combiner box under the same conditions.

B. *Optical Emission Spectroscopy*

Due to its robustness and design simplicity, optical emission spectroscopy has been used extensively to characterize copper arcs [3,4,5]. The arc temperature can be inferred from copper atoms released from the electrodes as they vaporize during the arc fault.

For this work, light emitted by the arc was focused into a TI300-UV-VIS fiber by a UVFS lens of f = 35 mm focal length, coupled to an Ocean Optics HR4000 Spectrometer at a data acquisition rate of $\upsilon = 100$ Hz. An Oriel argon pen lamp was used for wavelength calibration, and an Infrared Systems Development Co. IR-563 Blackbody and a Thorlabs SLS202L Tungsten lamp were used to correct the spectra for the wavelength-dependent detector efficiency. A test spectrum pre- and post-processing is shown in Figure 4.

Prior OES measurements used Cu I transitions at wavelengths of 465.1 nm, 510.5 nm, 521.8 nm [4,5]. Fig. 3, however, shows significant interferences at these wavelengths from impurities in the environment, limiting their usefulness. Therefore, temperature inference via a Boltzmann plot was completed by comparing four, spectrally isolated transitions with tabulated spectroscopic parameters, given in Table 2.

The linear distribution of relative populations is given in (1).

$$ln\left(\frac{I\lambda}{gA}\right) = \frac{-E_u}{kT} - ln\left(\frac{4\pi Z}{hcN_0}\right) \quad (1)$$

The measured line intensity, I, for a transition at wavelength, λ, can be inversely related to the temperature of the emitter, T, through the upper level energy, E_u, and spectroscopic constants including: the upper state degeneracy, g, the transition probability, A, and the Boltzmann constant, k. Improvements in measurement accuracy and sensitivity are ongoing, as more copper transitions with varying state energies are added to the Boltzmann plot. This method was chosen over spectral fitting as the gas composition in the field was unknown.

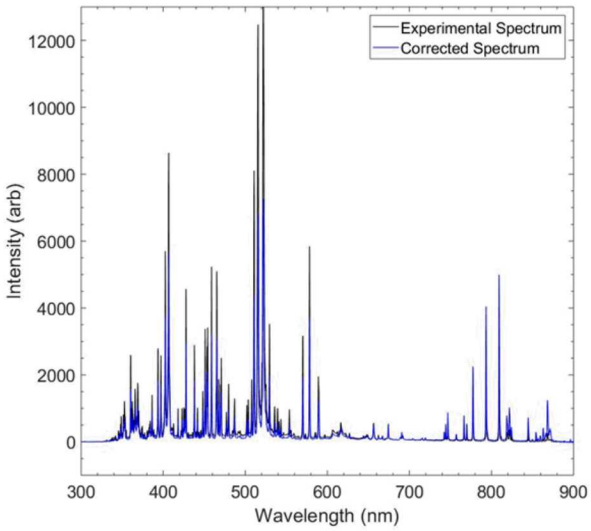

Fig. 4. Mean arc spectrum "as collected" (black) and corrected (blue) for an air-Cu arc sustained with V = 774 V_{DC} at G = 12.7 mm for t = 2 seconds.

TABLE II. CU I TRANSITIONS

Wavelength (nm)	g_2	E_1, cm^{-1}	E_2, cm^{-1}
570.0	12	13 245.4	30 783.7
578.2	6	13 245.4	30 535.3
793.3	6	30 535.3	43 137.2
809.3	6	30 783.7	43 137.2

C. IR Imaging

Imaging equipment was fielded in-line with the spectrometer. A Phantom v1212c camera collected high-speed visible images of the arc at 12,600 frames per second (fps), and a FLIR X6900sc high-speed, mid-wave infrared camera (MWIR), collected infrared images at 1004 fps. A representative image from each camera is shown in Figure 5 (a) for a snapshot of the arc using a visible high-speed camera and (b) for an image at the same interval using the high-speed infrared camera.

Spectra taken in the visible regime indicated that the arc-plasma radiates from the 0.3 to 0.9 μm. The infrared camera collected arc-environmental data from 3-5 μm.

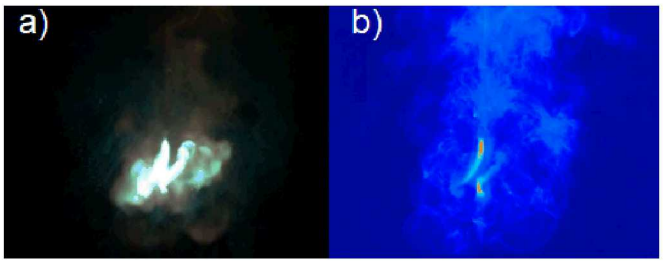

Fig. 5. Visble image of an arc flash (a) and infrared image of an arc flash (b) at t = 0.725 s during a test with an input source of V = 774 V_{DC} and G = 12.7 mm.

The frames were averaged during the arc test to identify a peak temperature of the gas surrounding the arc source. See Figure 6 (a) for the average of the photon counts (this provide an image that does not use the temperature calibrations of the camera). Figure 6 (b) depicts the average temperature of the arc in Kelvin.

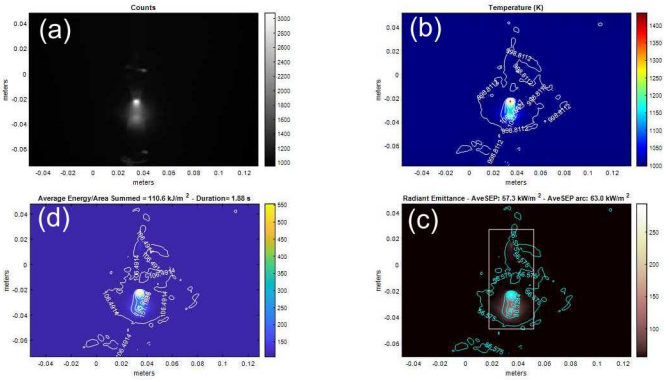

Fig. 6. Averaged photon counts (a), temperature (b), radiant emittance (c), and energy/area (d) of distribution maps inferred from averaged IR images of an arc fault. The arc fault occurs between two vertical Cu electrodes that sustained V = 774 V_{DC} at P = 264 kW_{peak}, separated by (a) G = 12.7 mm with an arc lasting t = 1.88 seconds.

Temperatures collected by MWIR camera can be related to radiance emittance from a blackbody assumption,

$$Re_0 = \sigma T^4, \quad (2)$$

where Re_0 (W/m^2), relates to the Stephen-Boltzmann constant, σ, and the temperature, T. However, the radiant emittance for real objects is reduced by the emissivity, ε, and the air transmittance, t_{air}, such that (2) is redefined as,

$$Re = t_{air}\varepsilon\sigma T^4. \quad (3)$$

The emissivity is difficult parameter to measure in a solid and it is even more difficult concept to relate to a plasma, therefore some work would be needed if emissivity should be attached to measuring plasma temperatures in the IR.

To determine the zone of influence the emissivity value is set to 1, that way the infrared radiation in the surroundings of

the arc is only considered. See Figure 6 (c) for the radiant emittance of the same measured case, and Figure 6 (d) for the fluence for (energy/area) this test lasting 1.88 seconds.

The zone of influence is calculated assuming that the arc flash can be modeled as a sphere. With this assumption it is possible to solve the radiometric equation for a distributed source:

$$Ed = \frac{\pi L a^2}{(a^2+ab+b^2)} \quad (4)$$

Where Ed is the irradiance at certain distance. For this problem the value is defined by the duration of the arc and solved for the case of unbearable pain [6]. L is the radiance of the arc, a is the radius of the sphere, and b is the distance where Ed is measured.

The duration of the arc is used to calculate the radiant emittance for unbearable pain, and it is possible to solve for the diameter (2b) of the zone of influence assuming a blackbody/graybody emission. Figure 7 shows the zone of emission for two cases with relatively small amounts of applied energy (vertical facing 0.5" and 2.0") with a small zone (less than a meter in diameter) of influence, and another example where the applied energy is 2 order of magnitude higher (vertical parallel 2.0") with a zone of influence of almost 12 meters in diameter.

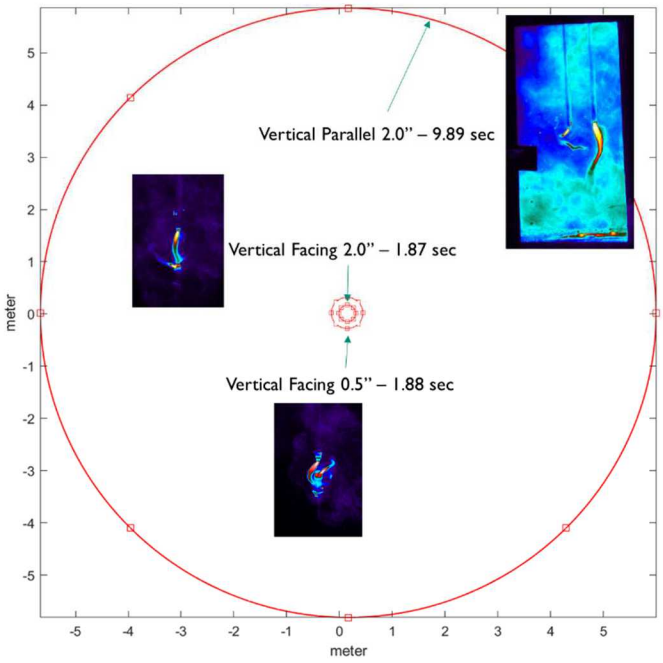

Fig. 7. The red circles are the minimum distance of unbearable pain for three different tests (geometry, gap, duration and applied energy)

The data from the IR camera needs to be compared to traditional radiometric methods, and this was done by looking at calorimeter mesaurements performed at the same time. Figure 8 shows the data comparison between the two methods and relates it to the applied energy to the test setup. Unfortunatelly the two instruments were not placed in the same location looking at the same part of the arc. For most of the tests, the IR camera was located about 30 degrees off normal and about 4 meters from the open box. For the two vertical facing 0.5" and 2.0" the IR camera was close to 10 degrees from normal, and about 3 meters from the box. The calorimeter for most of the tests was in close proximity, about 18 inches. This causes the instruments to see different emissions distributions and smoke distributions. This is important when comparing measurements. The results still show comparable results between the two methods. Further experiments need to be performed where the two instruments are placed at the same location looking at the same section of the arc.

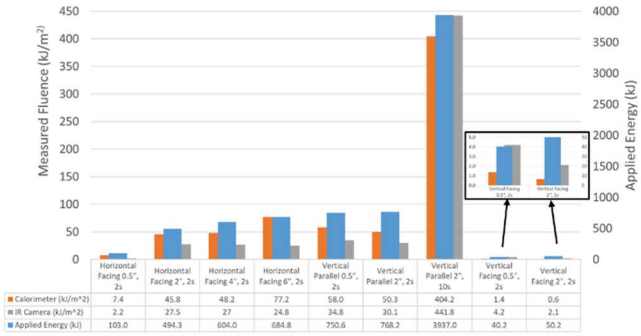

Fig. 8. Measured fluence from calorimeters and IR camera (left-axis) and applied energy (right) axis.

III. RESULTS AND DISCUSSION

Optical emission spectroscopy resolved that the majority of radiation in the UV and visible regime is spectral during an arc fault. Time-resolved arc temperatures inferred from the spectra are shown in Figure 9.

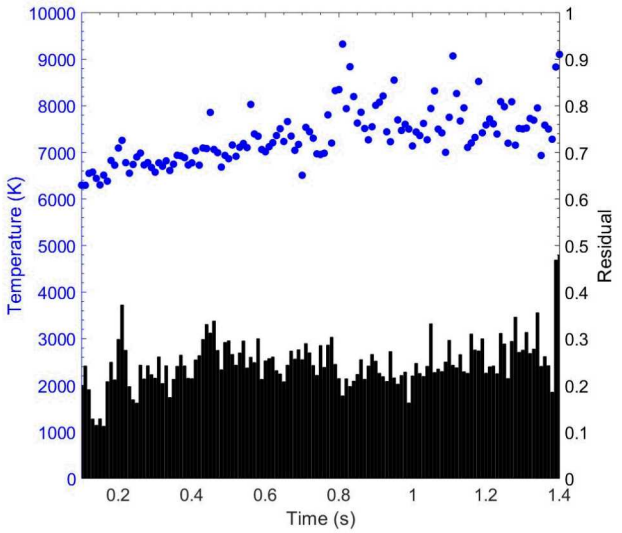

Fig. 9. Inferred temperature (blue circles) from a Boltzmann fit of the atomic copper transitions in the spectra and the residual (black bars) associated with each linear fit for an air-Cu arc with E_{App} = 40 kJ and G = 12.7 mm.

The arc temperature increases with time, and has a mean temperature, T_{mean} = 7349 ± 605 K. Contrastingly, the mean IR temperature fields were significantly lower, shown in Figure 6. Averaging the frames during the arc interval indicated peak average temperatures of T_{IR} = 1500 K, indicating a secondary phenomenon was being measured.

One hypothesis suggests energy from the arc-plasma heats molecules, like H_2O and CO_2, which then re-emit in the infrared. Further measurements of the emitted IR spectra are required to ascertain if the thermal emission is part of a continuum or related to molecular emissions.

Table 3 lists the inferred arc temperatures from the two vertical, pin-to-pin electrode configuration tests.

TABLE III. INFERRED ARC TEMPERATURES

Electrode Orientation	Gap (mm)	Applied Energy (kJ)	Mean Arc Temperature (K)	Std. Dev. (K)
Vertical, pin-to-pin	12.7	40	7349	605
Vertical, pin-to-pin	50.8	50	8013	658

The mean arc temperature increases with an increased applied energy and gap distance. OES measurements were taken for all arc-in-a-box configurations; however, the vertical, pin-to-pin configuration produced the most stable arc. The movement generated during the arc faults in the other two configurations increased the uncertainty of the mean arc temperature.

IV. SUMMARY AND CONCLUSIONS

OES and IR imaging have been fielded at the DTE solar park in July of 2019 to characterize dc arc faults generated from high-voltage, photovoltaic power systems. Arc temperature measurements were inferred from the time-resolved spectra by the linear Boltzmann method. This showed the feasibility of making time-resolved temperature measurements to understand arc evolution and produced a mean temperature of T_{mean} = 7349 ± 605 K for an arc with E_{App} = 40 kJ and gap spacing of 12.7 mm; additionally, a T_{mean} = 8013 ± 658 K was measured for an arc with E_{App} = 50 kJ and gap spacing of 50.8 mm. IR imaging provided mean temperature field measurements of the surrounding arc environment, which were significantly lower, T_{IR} = 1500 K, and suggest a secondary emissive process related to the transfer of arc energy.

V. ACKNOWLEDGMENT

The authors would like to acknowledge Ray Martinez for his help setting up of the equipment and Anthony Morabito for his help facilitating the onsite work.

This paper describes objective technical results and analysis. Any subjective views or opinions that might be expressed in the paper do not necessarily represent the views of the U.S. Department of Energy or the United States Government.

REFERENCES

[1] Augspurger Komm Engineering Inc., 2011, “Understanding arc flash hazards,,” http://akeinc.com/news/understanding-arc-flash-hazards.

[2] J. J. Lowke, “Simple theory of free-burning arcs,” in *Journal of physics D: Applied physics* 12 no. 11, p. 1873, 1979.

[3] C.H. Corliss, “Temperature of a copper arc." *NBS* 66, no. 1, p.5-12, 1962.

[4] I.L Babich, F.B. Viacheslav, N.V. Anatoly, “Shapes of spectral lines of nonuniform plasma of electric arc discharge between copper electrodes." In *AIP Conference Proceedings*, vol. 938, no. 1, pp. 252-257. American Institute of Physics, 2007.

[5] S. Franke, R. Methling, D. Uhrlandt, R. Bianchetti, R. Gati, and M. Schwinne. "Temperature determination in copper-dominated free-burning arcs." *Journal of Physics D: Applied Physics* 47, no. 1, p.015202, 2013.

[6] W. E. Baker, P. A. Cox, P. S. Westine, J. J. Kulesz and R. A. Strehlow, "Explosion Hazards and Evaluation," in Fundamental Studies in Engineering 5, Amsterdam - London-New York - Tokyo, Elsevier Scientific Publishing Company, pp. 548-561.